Biomedical Optics EXPRESS

High-speed multi-exposure laser speckle contrast imaging with a single-photon counting camera

Tanja Dragojević,[1,4,*] Danilo Bronzi,[2,4] Hari M. Varma,[1] Claudia P. Valdes,[1] Clara Castellvi,[3] Federica Villa,[2] Alberto Tosi,[2] Carles Justicia,[3] Franco Zappa,[2] and Turgut Durduran[1]

[1]*ICFO-Institut de Ciències Fotòniques, Av. Carl Friedrich Gauss, 3, Castelldefels (Barcelona), 08860, Spain*
[2]*Politecnico di Milano, Dipartimento di Elettronica, Informatione e Bioingegneria, Piazza Leonardo Da Vinci, 25, Milan, 20133, Italy*
[3]*Department of Brain Ischemia and Neurodegeneration, Insitute for Biomedical Reseach (IIBB), Spanish Research Council (CSIC), Insitut d'Investigacions Biomédical Research August Pi i Sunyer (IDIBAPS), Barcelona, Spain*
[4] *These authors contributed equally to the work.*
tanja.dragojevic@icfo.es

Abstract: Laser speckle contrast imaging (LSCI) has emerged as a valuable tool for cerebral blood flow (CBF) imaging. We present a multi-exposure laser speckle imaging (MESI) method which uses a high-frame rate acquisition with a negligible inter-frame dead time to mimic multiple exposures in a single-shot acquisition series. Our approach takes advantage of the noise-free readout and high-sensitivity of a complementary metal-oxide-semiconductor (CMOS) single-photon avalanche diode (SPAD) array to provide real-time speckle contrast measurement with high temporal resolution and accuracy. To demonstrate its feasibility, we provide comparisons between *in vivo* measurements with both the standard and the new approach performed on a mouse brain, in identical conditions.

OCIS codes: (030.5260) Photon counting; (040.1345) Avalanche photodiodes (APDs); (110.6150) Speckle imaging; (300.6480) Spectroscopy, speckle.

References and links

1. A. Devor, S. Sakaridžć, V. J. Srinivasan, M. A. Yaseen, K. Nizar, P. A. Saisan, P. Tian, A. M. Dale, S. A.Vinogradov, M. A. Franceschini, and D. A. Boas, "Frontiers in optical imaging of cerebral blood flow and metabolism," J. Cerebr. Blood F. Met. **32**, 1259–1276 (2012).
2. T. Durduran, R. Choe, W. B. Baker, and A. G. Yodh, "Diffuse optics for tissue monitoring and tomography," Rep. Progress Phys. **1**, 1–43 (2010).
3. V. Rajan, B. Varghese, T. G. van Leeuwen, and W. Steenbergen, "Review of methodological developments in laser doppler flowmetry," Lasers in medical science **24**, 269–283 (2009).
4. D. A. Boas and A. K. Dunn, "Laser speckle contrast imaging in biomedical optics," J. Biomed. Opt. **15**, 1–12 (2010).
5. A. K. Dunn, H. Bolay, M. A. Moskowitz, and D. A. Boas, "Dynamic imaging of cerebral blood flow using laser speckle," J. Cereb. Blood. Flow Metab. **21**, 195–201 (2001).
6. A. B. Parthasarathy, W. J. Tom, A. Gopal, X. Zhang, and A. K. Dunn, "Robust flow measurement with multi-exposure speckle imaging," Opt. Express **16**, 1975–1989 (2008).
7. A. B. Parthasarathy, S. M. Kazmi, and A. K. Dunn, "Quantitative imaging of ischemic stroke through thinned skull in mice with multi exposure speckle imaging," Biomed. Opt. Express **1**, 246–259 (2010).

#239632 Received 27 Apr 2015; revised 16 Jun 2015; accepted 7 Jul 2015; published 14 Jul 2015

8. S. Kazmi, S. Balial, and A. K. Dunn, "Optimization of camera exposure durations for multi-exposure speckle imaging of the microcirculation," Biomed. Opt. Express **5**, 2157–2171 (2014).
9. J. D. Briers and S. Webster, "Laser speckle contrast analysis (lasca): a nonscanning, full-field technique for monitoring capillary blood flow," J. Biomed. Opt. **1**, 174–179 (1996).
10. R. Bandyopadhyay, A. S. Gittings, S. S. Suh, P. K. Dixon, and D. J. Durian, "Speckle-visibility spectroscopy: A tool to study time-varying dynamics," Rev. Sci. Intrum. **76**, 093110 (2005).
11. J. D. Briers, G. Richards, and X. W. He, "Capillary blood flow monitoring using laser speckle contrast analysis (lasca)," J. Biomed. Opt. **4**, 164–175 (1999).
12. D. Bronzi, S. Tisa, F. Villa, S. Bellisai, A. Tosi, and F. Zappa, "Fast Sensing and Quenching of CMOS SPADs for Minimal Afterpulsing Effects," IEEE Photon. Technol. Lett. **25**, 776–779 (2013).
13. D. Bronzi, F. Villa, S. Tisa, A. Tosi, F. Zappa, D. Durini, S. Weyers, and W. Brockherde, "100 000 Frames/s 64 × 32 Single-Photon Detector Array for 2-D Imaging and 3-D Ranging," IEEE J. Sel. Top. Quantum Electron. **20**, 354–363 (2014).
14. F. Guerrieri, S. Tisa, A. Tosi, and F. Zappa, "Two-dimensional SPAD imaging camera for photon counting," IEEE Photonics J. **2**, 759–774 (2010).
15. S. Yuan, "Sensitivity, noise and quantitative model of laser speckle contrast imaging," ProQuest (2008).
16. C. P. Valdes, H. M. Varma, A. K. Kristoffersen, T. Dragojević, J. P. Culver, and T. Durduran, "Speckle contrast optical spectroscopy: A non-invasive, diffuse optical method for measuring microvascular blood flow in tissue," Biomed. Opt. Express **5**, 2769–12784 (2014).
17. H. M. Varma, C. P. Valdes, A. K. Kristoffersen, J. P. Culver, and T. Durduran, "Speckle contrast optical tomography: A new method for deep tissue three-dimensional tomography of blood flow," Biomed. Opt. Express **5**, 1275–1289 (2014).
18. L. Hillesheim, J. Müller "The photon counting histogram in fluorescence fluctuation spectroscopy with non-ideal photodetectors," Biophys. J. **85**, 1948–1958 (2003).
19. C. Ayata, A. K. Dunn, Y. Gursoy-Özdemir, Z. Huang, D. A. Boas, and M. A. Moskowitz, "Laser speckle flowmetry for the study of cerebrovascular physiology in normal and ischemic mouse cortex," J. Cereb. Blood Flow Metab. **24**, 744–755 (2004).
20. R. Bi, J. Dong, and K. Lee, "Deep tissue flowmetry based on diffuse speckle contrast analysis," Opt. Express **21**, 22854–22861 (2013).
21. R. Bi, J. Dong, and K. Lee, "Multi-channel deep tissue flowmetry based on temporal diffuse speckle contrast analysis," Opt. Lett. **38**, 1401–1403 (2013).

1. Introduction

Non-invasive, optical imaging of blood flow in general, and in particular cerebral blood flow (CBF) has many applications in studying both the normal and pathopshysiological brain [1]. Diffuse correlation spectroscopy (DCS) [2], laser Doppler flowmetry [3], laser speckle contrast imaging (LSCI) [4] are some of the optical methods based on the spatio-temporal statistics of the laser speckles that are used to measure blood flow in the microvasculature.

In LSCI, an *in vivo* imaging technique, full-field illumination is used for measurement of blood flow in real time using two-dimensional array detectors such as CMOS or CCD cameras [5]. The blurring of fluctuating speckles during the brief, yet significantly long, exposure time of the camera is quantified and compared to a physical model. To date, the bulk of LSCI work relied on the use of a single-exposure time, which allowed fairly simple and inexpensive experimental set-up that can measure the relative changes in CBF with high spatio-temporal resolution.

The use of single exposure data limits the LSCI to relative measurements and makes it vulnerable to systematic errors because of deviations from the physical theories due to the presence of static scatterers. Multi-exposure laser speckle imaging (MESI) is an attempt to resolve these problems by using multi-exposure time data [6–8]. The main drawback of MESI is due to the additional time necessary for acquiring different exposure time sequences. Therefore, it lacks the temporal resolution necessary for imaging rapid changes in blood flow, preventing real-time *in vivo* measurements to be performed and thus leading to a trade-off between accuracy, resolution and speed.

In order to overcome these limitations, in this paper, we exploit the unique characteristics of a a single-photon avalanche diode (SPAD) array such as no readout noise, high-speed and single-

#239632 Received 27 Apr 2015; revised 16 Jun 2015; accepted 7 Jul 2015; published 14 Jul 2015

photon sensitivity performance. These allow us to achieve real-time multi-exposure speckle contrast measurement with high temporal resolution, even at low light intensity levels and at a high frame rate. The lack of readout noise and fast frame-rate capability of the SPAD chip also allows for a new acquisition scheme, herein called as single-shot acquisition MESI (sMESI), which can compute the whole set of multi-exposure images from a single acquisition at the shortest exposure time without significant inter-frame dead time. To validate our technique, we have performed measurements on a tissue-like phantom followed by an *in vivo* mouse measurement.

The paper is structured as follows: Section 2 addresses the theory of multi-exposure speckle imaging and describes the structure and the working principles of the SPAD chip. Furthermore, we discuss the new acquisition method, its validation and comparison with the standard approach. In Section 3, we discuss the results from different sets of experimental data. Finally, in Section 4 we outline the main advantages and drawbacks of the proposed methods and of the system.

2. Methods

2.1. Single and multi-exposure laser speckle contrast imaging

A laser speckle pattern is a random interference pattern produced by the coherent addition of scattered laser light with slightly different path lengths [9]. One source of fluctuations in the speckles is the presence of dynamic scatterers, like moving red cells in the blood. The statistical properties of the scatterer dynamics are reflected in the speckle fluctuations which, in case of LSCI, are quantified by a statistical quantity called speckle contrast, (κ), defined as the ratio of the standard deviation (σ) to the mean intensity ($\langle I \rangle$) in a local region [4].

Furthermore, the square of speckle contrast is related to normalized electric field autocorrelation function of the scattered field, ($g_1(\tau)$) [10]:

$$\kappa^2 = \frac{\sigma^2}{\langle I \rangle^2} = \frac{2\beta}{T}\int_0^T g_1^2(\tau)\Big(1-\frac{\tau}{T}\Big)d\tau \tag{1}$$

where β is related to the number of speckles that are detected by each individual pixel, T is the exposure time of the camera, and τ is the correlation time. In case of single scattering, the normalized field autocorrelation assumes the form of $g_1(\tau) = \exp(-T/\tau_c)$; where τ_c is the correlation time for the speckles and is connected to blood flow as $\tau_c = 1/v$, where v is velocity of the scatterers [11]. Inserting this form into Eq. (1) and integrating, the speckle contrast becomes:

$$\kappa^2(T,\tau_c) = \beta\frac{e^{-2(T/\tau_c)} - 1 + 2(T/\tau_c)}{2(T/\tau_c)^2}\ . \tag{2}$$

In the presence of static scatterers Eq. (2) needs to be modified [6]:

$$\kappa^2(T,\tau_c) = \beta\rho^2\frac{e^{-2(T/\tau_c)} - 1 + 2(T/\tau_c)}{2(T/\tau_c)^2} + 4\beta\rho(1-\rho)\frac{e^{-(T/\tau_c)} - 1 + (T/\tau_c)}{(T/\tau_c)^2} + v_{noise} \tag{3}$$

where $\rho = I_f/(I_f + I_s)$, I_f and I_s are contributions from dynamic and static scattered light respectively and v_{noise} is variable that accounts for experimental error. In absence of static scatterers, ($\rho = 1$), Eq. (3) reduces to Eq. (2).

In the following, we will demonstrate the single-shot acquisition MESI using the data acquired by the SPAD camera and by making use of speckle contrast given in Eq. (3).

#239632 Received 27 Apr 2015; revised 16 Jun 2015; accepted 7 Jul 2015; published 14 Jul 2015

2.2. *Single-photon avalanche diode (SPAD) array*

The main process exploited in a SPAD is the impact of ionization mechanism. However, differently from avalanche photodiodes (APDs), where the ionization mechanism is deployed to produce a linear amplification of the photocurrent, a SPAD produces, upon the absorption of a photon, a high current pulse (milliampere) with sub-nanosecond leading edge, thus ensuring precise time-tagging of the photon arrival. This is a consequence of the fact that a SPAD is basically a p-n junction, that is reverse-biased well above the breakdown voltage. At this bias, the electric field in the depletion layer is so high that a single injected carrier can trigger a self-sustaining avalanche current, that is sensed and quenched by a proper front-end circuit, which also generates a digital pulse synchronous with the current sensing [12]. This implies that each photon is directly converted into a 1-bit count and, therefore, unlike CCD and CMOS imagers, the contribution of readout noise is completely removed. Correspondingly, no limitation on minimum integration time, due to signal-to-noise ratio (SNR) degradation, is set and very high frame rate acquisition becomes feasible. Moreover, if an application requires long integration times, e.g. T_{INT} seconds, it is possible to accumulate N frames, each lasting T_{FRAME} (Fig. 1). When negligible inter-frame time and a very short minimum frame time can be achieved, the resulting dynamic range of the sensor dramatically increases [13]. In principle, the same strategy could be applied to CCDs and CMOS sensors, but the dominant contribution of the readout noise at short integration time, would inevitably cause signal-to-noise (SNR) degradation [14]. This feature is of great concern for MESI, since speckle data are acquired for a wide range of exposure times (10 μs up to 80 ms), where the lowest value is typically tens of μs. At such short exposures, the data will exhibit a low SNR in the presence of high readout noise.

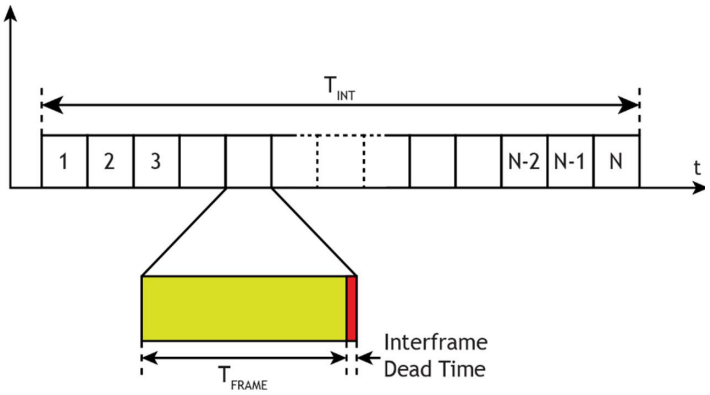

Fig. 1. Typical acquisition scheme for the adopted SPAD array: given the absence of readout noise and short inter-frame dead time, longer integration time can be obtained by accumulating several shorter frames. The dynamic range is correspondingly increased.

The SPAD sensor chip used for this study is an array of 64×32 SPAD pixels and integrated electronics fabricated in a high-voltage 0.35 μm CMOS technology. Each pixel is a round SPAD, with a 30 μm active-area diameter, and includes an analog quenching circuit front-end, processing circuitry and data readout [13]. At room temperature, the SPAD has one of the best ever reported dark noise performance (100 cps). The system has an extended dynamic range of 110 dB at 100 fps and a maximum frame-rate of 100,000 fps. The dead time is fairly short, 35 ns, corresponding to maximum count rate of $\sim$28 Mcps. This performance ensures photon-shot noise limited acquisition, further increasing the accuracy of the measurements.

#239632 Received 27 Apr 2015; revised 16 Jun 2015; accepted 7 Jul 2015; published 14 Jul 2015

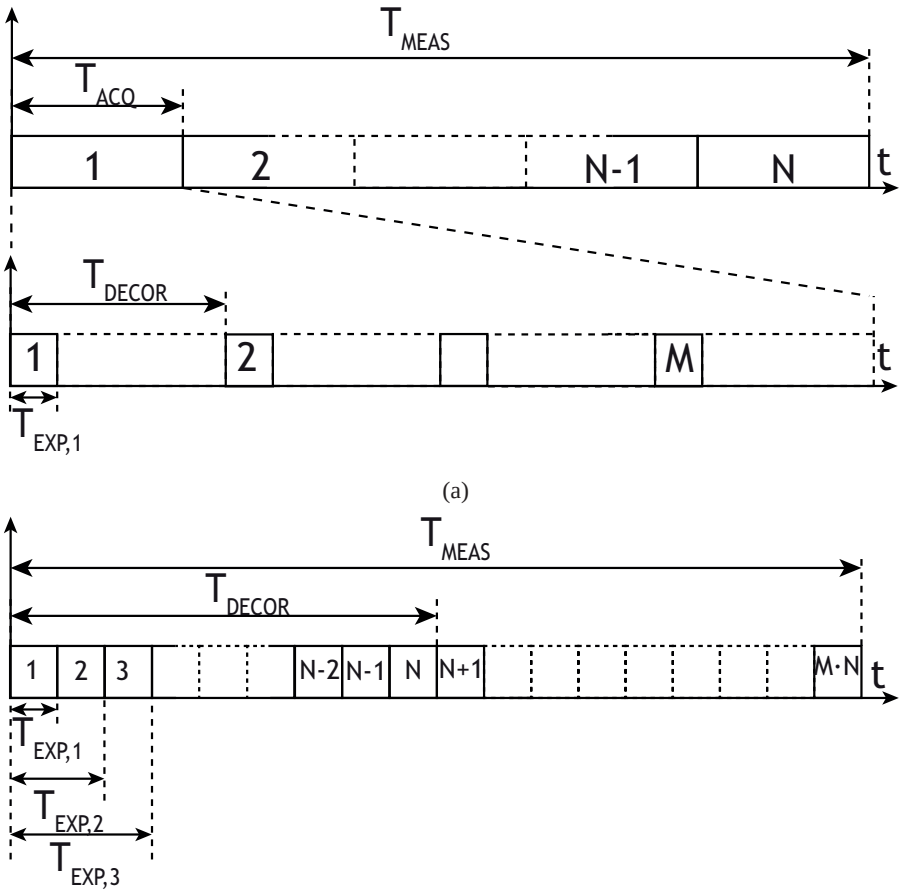

Fig. 2. Acquisition protocol for (a) standard and (b) sMESI methods. $T_{EXP,i}$ is the i-th exposure time; T_{DECOR} is the decorrelation time. T_{ACQ} is the acquisition of a single exposure time, while N is the number of exposure times (T_{FRAME}) needed and M is the number of images for each exposure.

2.3. Single-shot acquisition multi-exposure speckle imaging with single photon avalanche diode array

The particular acquisition protocol is important when considered in relationship to functional imaging with small animal models, where data is acquired for long time. In the standard MESI approach [6], where a laser source is gated with an acousto-optic modulator or in case of gated-CCD the camera itself is gated, N different exposures ($T_{EXP,i}$, i=1,...,N), ranging from tens of microseconds to tens of milliseconds are employed. The time in between each exposure is also in the order of tens of milliseconds and it depends on the speckle decorrelation time (T_{DECOR}) [7,8]. The acquired data over M images are processed to calculate the speckle contrast and then averaged for each exposure time (Fig. 2(a)). Since data is acquired in discrete sets of exposure time ($T_{ACQ} = M \cdot T_{DECOR}$), the whole measurement process is time consuming ($T_{MEAS} = N \cdot T_{ACQ}$) and the longer the duration is, the higher the probability that data will be affected by physiological and experimental changes.

#239632 Received 27 Apr 2015; revised 16 Jun 2015; accepted 7 Jul 2015; published 14 Jul 2015

To overcome this limitation, we take advantage of the readout-noise-free images from the SPAD array to increase the acquisition speed and instead of multiple exposures (i.e. one exposure acquisition after the other), a single high-speed acquisition (short exposure time) is performed. In post-processing, the frames are then summed to obtain N different equivalent exposure times ($T_{EXP,N} = \sum_{i=1}^{N} T_{FRAME}$), and for each processed exposure time the speckle contrast is computed. As shown in Fig. 2(b), T_{FRAME} is chosen so that in a single decorrelation interval, it is possible to acquire N exposure times, then the acquisition speed improves by a factor N.

As an example, let us consider that we want to use twenty-one different exposure times, and for each one, 500 images are averaged with a decorrelation time equal to 20 ms (e.g. 50 fps). When using the standard approach, the total measurement time is $T_{MEAS} = M \cdot N \cdot T_{DECOR} = 210$ s, that is about 3.5 minutes. Conversely, with the new approach, choosing a frame time equal to $T_{FRAME} = T_{DECOR}/N = 200\ \mu$s, we can acquire the same amount of images per exposure time in only $T_{MEAS} = M \cdot T_{DECOR} = 10$ s. Even further, the advantages can be greater. Thanks to the higher frame rate capability, we are able to choose a frame time as short as 10 μs. In such a situation, we are able to generate $N = T_{DECOR}/T_{FRAME} = 10000$ equivalent exposure times. As a result, we are not only able to drastically reduce the measurement duration but also to generate more points per acquisition, thus increasing the precision of τ_c estimation.

2.4. Phantom and in vivo measurements

To validate the SPAD for LSCI use and for data acquisition with sMESI, we have used a phantom of 1% solution of Lipofundin 20% (B. Braun, Spain) in water with optical properties for scattering $\mu_s' = 10.3$ cm^{-1} and absorption $\mu_a = 0.04$ cm^{-1}. A continuous-wave temperature controlled laser diode (L785P090 Thorlabs, 785 nm, 90 mW) was used for homogeneous full-field illumination.

The experimental setup, shown in Fig. 3(a), was used for measurements of the tissue simulating phantom and the animal. Data was acquired over multi-exposure times from 200 μs up to 2000 μs in steps of 200 μs, in total 10 exposure times for phantom measurement for both methods.

Furthermore, to demonstrate the feasibility of single-shot acquisition MESI, *in vivo* measurements, an adult male C57/BL6 mouse (30 g of body weight) was used. The animal was initially anesthetized with 4% isoflurane in O_2:N_2O (30:70), which was reduced to 1% isoflurane for maintenance, once the mouse was moved to the stereotaxic frame, as shown in Fig. 3(a). Body temperature was kept at 37 ^{o}C by a heating blanket and animal scalp was removed. A Teflon ring was attached to the skull using dental cement and filled with mineral oil to prevent the skull from drying out during the measurement.

Two types of challenges were introduced to alter the global cerebral blood flow. First challenge was hypercapnia, where carbon dioxide (CO_2) concentration was increased, thus leading to increase in blood flow. The second challenge was hyperoxia, where oxygen (O_2) concentration was increased, in order to decrease blood flow. The protocol of the whole measurement lasted 30 minutes. As shown in Fig. 3(b): we first took baseline measurements with both methods, followed by the CO_2 challenge (20% O_2 + 75% N_2O + 5% CO_2). Then, we waited 5 minutes for the animal to recover, and O_2 challenge (100% O_2) was introduced. At the end of measurements the animal was sacrificed and the biological zero was imaged. All the multi-exposures were taken with exposure times from 200 μs up to 20000 μs, in total 21 exposure times for both methods.

#239632 Received 27 Apr 2015; revised 16 Jun 2015; accepted 7 Jul 2015; published 14 Jul 2015

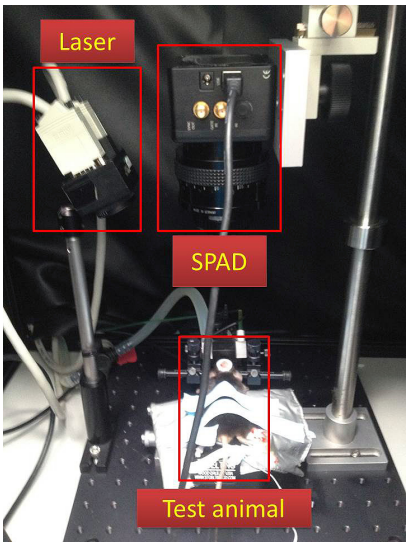

(a)

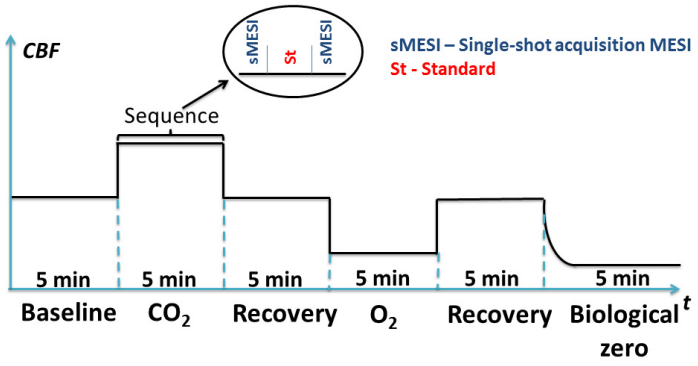

(b)

Fig. 3. Measurement protocol and setup: (a) *In vivo* measurement setup, showing laser, SPAD camera and animal; (b) Protocol for *in vivo* measurement, showing how data was sequentially acquired. Each sequence had a single-shot acquisition MESI (sMESI) and standard acquisition (St).

2.5. Data processing and fitting

Speckle contrast was computed in a predefined region of interest (ROI) at each pixel over all frames. In order to account for the shot noise, we adopt the noise correction method explained in Refs. [15–17]. The contribution due to shot noise, $\kappa_s=1/\langle I\rangle$, is subtracted from the computed speckle contrast. Dark noise may also lead to systematic error, which is negligible for this low exposure time used in this study since the dark count level is at 100 cps. The readout noise is non-existent. We have previously shown that these sources of noise can also be taken into account if need be [16].

Furthermore, in the case of count rates closer to the saturation level, it is possible to do a correction for the dead time [18]. Since the count rate levels are well below saturation in this study, we did not take this into account. All additional noises that were not considered were

#239632 Received 27 Apr 2015; revised 16 Jun 2015; accepted 7 Jul 2015; published 14 Jul 2015

incorporated to the v_{noise} while fitting for data.

In MESI often, the speckle contrast is computed in spatial domain, using a number of statistically independent pixels in a square window (5x5 or 7x7). Here, instead, we compute the speckle contrast in temporal domain by making use of uncorrelated images spaced appropriately in time to let the speckle field decorrelates. The limits of validity of this approach is well known [4].

3. Results

A tissue mimicking phantom was used to test the new (sMESI) method in comparison to the standard method. Temporal speckle contrast was calculated using the intensity and the variance for each pixel (2048 pixels) over 1000 images. Figure 4 shows the intensity and speckle contrast over different exposure times. We note that for the shortest exposure time (200 μs), from which all other exposure times were build up, the maximum count rate was 0.6 Mcps. As it can be seen, the two methods are in close agreement. The mean difference between these two methods for intensity is 0.4 $\pm$ 0.1 %, and for speckle contrast is 3.4 $\pm$ 1.3 % .

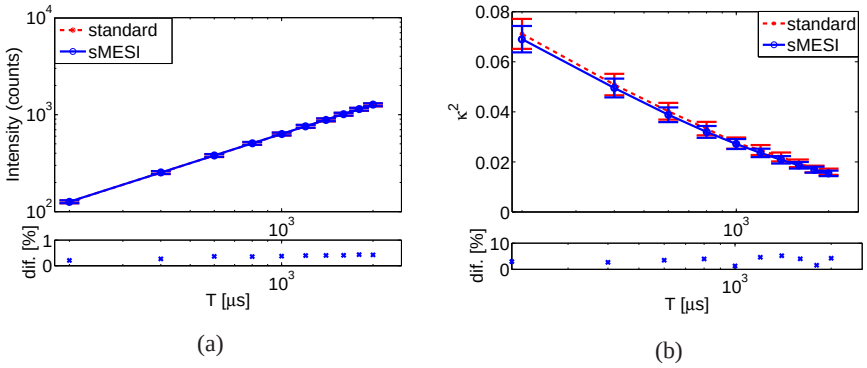

(a) (b)

Fig. 4. Measured (a) intensity and (b) speckle contrast versus exposure time for the liquid phantom measurement. Standard data (dashed), and new single-shot acquisition data (solid line) are shown. The mean difference from intensity is 0.4 $\pm$ 0.1 % whereas, speckle contrast mean difference is 3.4 $\pm$ 1.3 %.

After demonstrating the validity of the measurements in the phantom, we translated the measurements to *in vivo*. The temporal speckle contrast calculation was performed for each pixel over 500 images and averaged for the region of interest of 8×5 pixels. Figure 5 shows a representative SPAD image where major vessels are visible.

Figure 6 shows the intensity and the temporal speckle contrast versus the exposure time, as well as the difference between two methods during the baseline period for both standard and sMESI. The mean difference in intensity is 0.95 $\pm$ 0.35% and 8.8 $\pm$ 6.5% for the speckle contrast between these two methods. The baseline speckle contrast was fitted using the theoretical model given in Eq. (3) and normalized to the mean value as shown in Fig. 7. The mean residual between the fit and the data for the standard method is 9.2 $\pm$ 0.2% and for sMESI is 9.2 $\pm$ 0.1%. The fitted values are also in good agreement between both models. The maximum count rate was 1 Mcps for the shortest exposure time (200 μs) from which all other exposure times were built up.

In Table 1 and Table 2, all fitted values of τ_c and cerebral blood flow (CBF) for the single-shot acquisition and the standard method are shown. Overall, we see that τ_c obtained from two methods are comparable. Furthermore, assuming that $\tau_c \sim 1/v$, and CBF$\sim v$, we compute CBF

#239632 Received 27 Apr 2015; revised 16 Jun 2015; accepted 7 Jul 2015; published 14 Jul 2015

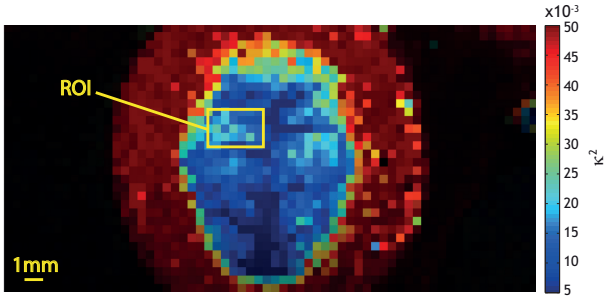

Fig. 5. An *in vivo* image of the mouse brain with the selected region of interest (ROI, 8×5 pixels) of 4×2.5mm. The Teflon ring appears as a halo around the exposed brain. Field of view was approximately 3×1.5 cm.

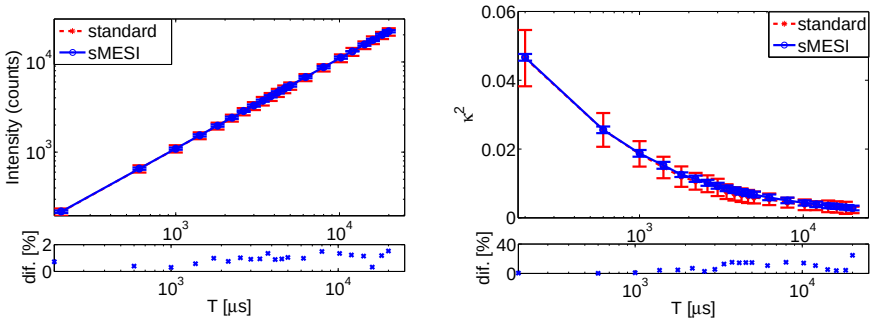

Fig. 6. Mouse measurements for (a) intensity and (b) speckle contrast as a function of exposure time are shown. The dashed line is the standard method and the solid line is the single-shot acquisition method. The mean difference between these two methods is for the intensity $0.95 \pm 0.35\%$, and for the speckle contrast $8.8 \pm 6.5\%$.

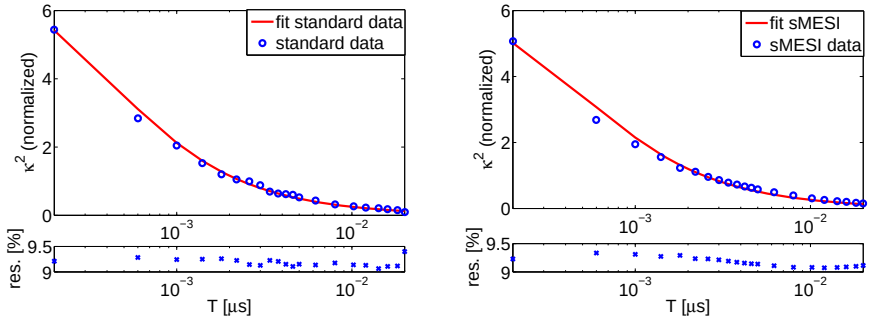

Fig. 7. Fitted data from (a) standard and (b) single-shot acquisition from the baseline measurements. The mean residual between the theory and the experiment from the standard method is $9.2 \pm 0.1\%$ and for standard method is $9.2 \pm 0.2\%$.

#239632 Received 27 Apr 2015; revised 16 Jun 2015; accepted 7 Jul 2015; published 14 Jul 2015

changes for the hypercapnia (Table 1) and hyperoxia (Table 2). As shown in the tables and in Fig. 8, the changes in CBF during each challenge match the expectations; hypercapnia with a CO_2 increase causes an expected decrease for τ_c and an increase in CBF; and hyperoxia i.e. O_2 increase causes an increase in τ_c and a decrease in CBF. Biological zero, i.e. τ_c measured after sacrifice (Table 2), was subtracted from all the measurements and the values were normalized to the baseline measured before each challenge. As it can be seen the single-shot acquisition and standard method are in close agreement.

Table 1. Fitted values for τ_c and cerebral blood flow with biological zero subtraction before, during and after hypercapnia.

Challenge	$\tau_c[s]$		Cerebral blood flow[%]	
	sMESI (10^{-4})	Standard(10^{-4})	sMESI	Standard
Baseline	3.80 ± 0.4	3.41 ± 0.32	100	100
CO_2	3.10 ± 0.29	3.04 ± 0.26	121.6 ± 2.0	112.1 ± 4.6
Recovery	3.17 ± 0.33	3.10 ± 0.23	118.9 ± 1.6	109.7 ± 3.6

Table 2. Fitted values for τ_c and cerebral blood flow with biological zero subtraction before, during and after hyperoxia. The biological zero values are also shown in this table since the animal was sacrificed after hyperoxia.

Challenge	$\tau_c[s]$		Cerebral blood flow[%]	
	sMESI (10^{-4})	Standard(10^{-4})	sMESI	Standard
Recovery (Baseline)	3.17 ± 0.33	3.10 ± 0.23	118.9 ± 1.6	109.7 ± 3.6
O_2	3.23 ± 0.33	3.24 ± 0.24	98.3 ± 4.0	95.8 ± 4.7
Recovery	2.83 ± 0.26	2.89 ± 0.24	112.0 ± 3.3	107.5 ± 4.3
Biological zero	259 ± 4	519 ± 89	0	0

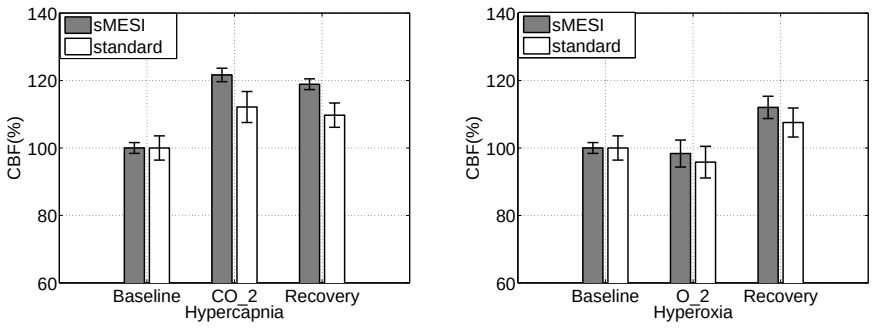

(a) (b)

Fig. 8. Bar plots for the changes in cerebral blood flow (a) for the hypercapnia challenge normalized to the baseline period immediately prior to hypercapnia (Table 1) and (b) for the hyperoxia challenge to the baseline period immediately prior to hyperoxia after the hypercapnia (Table 2).

#239632 Received 27 Apr 2015; revised 16 Jun 2015; accepted 7 Jul 2015; published 14 Jul 2015

4. Discussion

We have presented a new, high-frame rate single photon avalanche diode (SPAD) array for laser speckle contrast imaging. Furthermore, we have proposed and demonstrated a new method for fast multi-exposure data acquisition. Single-shot acquisition MESI (sMESI) is able to acquire thousands of frames rapidly with negligible dead time between frames, and, with post-processing of the data, to simulate multi-exposure data.

To demonstrate that the SPAD and sMESI are able to measure speckle contrast, a measurement on a tissue mimicking phantom was shown. The intensity and speckle contrast in liquid phantom from both approaches were in close agreement with mean difference of $0.4 \pm 0.1\%$, and $3.4 \pm 1.3\%$ respectively. This shows that both approaches generate equivalent data in ideal conditions.

After proving this, measurements were translated to the mouse brain. As described in Section 3, we have first compared both methods during the baseline period, again with a close agreement between both methods for both the intensity ($0.95 \pm 0.35\%$) and the speckle contrast ($8.8 \pm 6.5\%$). As expected, the differences are a bit larger for the *in vivo* case due physiological changes between two sets of acquisition.

Then all measurements were fitted with a theoretical model, this is enabled by both MESI and sMESI which showed good agreement between methods and with previously reported values [8]. Furthermore, cerebral blood flow changes due to two challenges (hypercapnia and hyperoxia) also showed agreement between two methods and with previously reported values [19]. Overall, these results demonstrate that the new approach can provide equivalent data as standard MESI at a significantly shorter time.

We note that the SPAD array provides good signal-to-noise-ratio even for the lowest exposure times that were utilized, it can readily be gated and has a high effective dynamic range. Therefore, it is suitable for multi-exposure speckle contrast imaging. Our work demonstrates this point. However, we go further and utilize the absence of readout noise, the negligible inter-frame dead-time and the resulting high frame rate acquisition to propose and demonstrate sMESI.

The standard CMOS manufacturing employed for this SPAD array allows to achieve both single-photon sensitivity, very low noise and very high (hundreds of kfps) frame rates. The current SPAD array has been designed in a scaled technology ($0.30\ \mu$m) that allows for low noise SPADs, but at the cost of a large pixel pitch ($150\ \mu$m). This implies a limited number of pixels (2048) and a relative slow readout electronics (100 MHz readout clock frequency). In deep sub-micron technologies ($< 0.18\ \mu$m), the pixel pitch could be reduced (down to about $30\ \mu$m) and consequently the number of pixels can be increased to achieve a higher spatial resolution (around 20 kpixels) using the same area. The maximum frame rate can still be kept comparable or even higher because these more scaled technologies also allow us to integrate faster transistors (1 GHz readout clock frequency). In the near future ($\sim$one year) it is envisioned that a SPAD array with this configuration will be available. We note that the production technologies are well known and in the longer term (few years), as applications similar to the work presented here arise, we expect that arrays with similar pixel density as already existing CCD/CMOS cameras will be available.

Moreover, we note that there are some limitations due to low quantum efficiency for our wavelength (785 nm). Next generation of CMOS SPAD arrays are also expected to maintain the uniformity so far achieved and possibly provide even higher quantum efficiency in the near-infrared (700-900 nm) range which is a current limitation [13].

These new arrays will not only improve the single-shot acquisition measurements at lower exposure times, but it will also allow to use SPAD array for speckle contrast spectroscopy (SCOS) and tomography (SCOT) using point sources and large source-detector separations [16,

#239632 Received 27 Apr 2015; revised 16 Jun 2015; accepted 7 Jul 2015; published 14 Jul 2015

17, 20, 21]. As a matter of fact, we envision that these larger SPAD arrays are going to be more and more disruptive and could eventually reach a timing resolution and quantum efficiency enabling diffuse correlation spectroscopy measurements [2].

5. Conclusion

We have introduced a new multi-exposure laser speckle contrast imaging approach using a state-of-the-art high frame-rate SPAD array chip. We have demonstrated that the high frame, single-photon counting sensitivity and the negligible inter-frame dead-time allows for single-shot acquisition of multi-exposure laser speckle data. This improved performance will open the way to further improvements both in the methodology and in the detector design.

Acknowledgments

The project was funded by Fundació Cellex Barcelona, Ministerio de Economía y Competitividad (PHOTOSTROKE), l'Obra Social "la Caixa"(LlumMedBCN) and LASERLAB-EUROPE III (Bioptichal).

#239632 Received 27 Apr 2015; revised 16 Jun 2015; accepted 7 Jul 2015; published 14 Jul 2015